



Low Cost, Recyclable and Magnetic *Moringa Oleifera* Leaves for Chromium(VI) Removal From Water

Daniel Masekela¹, Tunde L. Yusuf¹, Nomso C. Hintsho-Mbita^{2,3} and Nonhlangabezo Mabuba^{1*}

¹ Department of Chemical Sciences (formerly known as Applied Chemistry), University of Johannesburg, Johannesburg, South Africa, ² Department of Chemistry, University of Limpopo, Polokwane, South Africa, ³ Department of Science Innovation/National Research Foundation (DSI/NRF) Centre of Excellence in Strong Materials, Johannesburg, South Africa

OPEN ACCESS

Edited by:

Ulises Javier Jauregui-Haza,
Santo Domingo Institute of
Technology, Dominican Republic

Reviewed by:

Abdul Waheed,
King Fahd University of Petroleum and
Minerals, Saudi Arabia
Shamsuddeen Haladu,
Imam Abdulrahman Bin Faisal
University, Saudi Arabia

*Correspondence:

Nonhlangabezo Mabuba
nmabuba@uj.ac.za

Specialty section:

This article was submitted to
Water and Human Health,
a section of the journal
Frontiers in Water

Received: 08 June 2021

Accepted: 10 January 2022

Published: 08 April 2022

Citation:

Masekela D, Yusuf TL,
Hintsho-Mbita NC and Mabuba N
(2022) Low Cost, Recyclable and
Magnetic *Moringa Oleifera* Leaves for
Chromium(VI) Removal From Water.
Front. Water 4:722269.
doi: 10.3389/frwa.2022.722269

Chromium(VI) a heavy metal by nature, is one of the most toxic metals in the environment. We recently reported functionalized *Moringa Oleifera* (FMO) leaves as a low cost and efficient adsorbent for the removal of Cr(VI) and bacterial from water, as a continuation, we report the incorporation of magnetic nanoparticles (Fe₃O₄) with previously studied FMO for Cr(VI) removal from aqueous solution. Iron oxide due to its magnetic properties has been shown to assist in the recovery of its adsorbents. In this study, *in-situ* co-precipitation synthesis of iron nanoparticles onto FMO was employed. During chemical precipitation, the iron precipitate tends to cover the FMO thus forming some outer-shell coating of magnetite on the surface of FMO. The Fe₃O₄/FMO was characterized using XRD, FTIR, SEM, BET, TGA and Zeta potential. FTIR results showed a new developed intense peak at 685.6 cm⁻¹ for Fe-O stretching, indicating successful incorporation of Fe₃O₄ nanoparticles onto FMO. Powder XRD was further use to confirm the formation and further indicated that the structure of FMO was still intact even after the Fe₃O₄ incorporation. The adsorption conditions such as pH, dosage, time and concentration were optimized to 2, 0.15 g, 25 min and 20 mg/L, respectively. The adsorbent was selective toward Cr(VI) since 99% was removed in the presence of interfering ions (20–100 mg/L). The adsorbent (Fe₃O₄/FMO) could also be reused up to 4 times with a percentage Cr(VI) removal of >80% in the 4th cycle. Adsorption kinetics studies obeyed pseudo second-order model, suggesting a chemical interaction mechanism (chemisorption) between Fe₃O₄/FMO and Cr(VI). Therefore, the adsorbent has shown that it can be used for selective removal of Cr(VI) from wastewater and potentially other heavy metals as well.

Keywords: magnetite nanoparticle (MNPs), *Moringa Oleifera*, Chromium(VI), UV-vis spectrophotometer, adsorbents

INTRODUCTION

The release and leaching of heavy metals into our water stream caused by industrialization and urbanization has had a devastating effect on to the environment. One of the heavy metals that is a serious health problem is chromium (Periyasamy et al., 2019). In aqueous solution, chromium exists in two forms, either as trivalent [Cr(III)] or hexavalent [Cr(VI)]. The trivalent oxidation state, Cr(III) is an essential element which is required by our bodies for metabolic activities. Whereas,

Cr(VI) has been shown to be one of the most toxic element since it has a high mobility and solubility, as it enters through our cell membranes as CrO_4^{2-} or HCrO_4^- to oxidize biomolecules (Cieślak-Golonka, 1996; Pellerin and Booker, 2000; Krishna et al., 2004). The World Health Organization (WHO) from their guidelines have set the maximum limit for Cr(VI) to be 0.10, 0.25 and 0.05 mg/L in surface, industrial and drinking water (water for consumption), respectively (Krishnani et al., 2013; Kera et al., 2017). In order to adhere with the recommended limits, it is imperative that wastewater from industries are treated to lower the Cr(VI) concentration in an effort to get it to the allowed permissible levels before being released into the environment. Several water treatment techniques including ion exchange, membrane separation, precipitation, coagulation and adsorption have been used for Cr(VI) removal from water (Kurniawan et al., 2006; Saha et al., 2011; Nguyen et al., 2013; Kalidhasan et al., 2016). Unfortunately, a majority of these techniques suffer from several drawbacks such as incomplete Cr(VI) removal, high operational cost, low selectivity, not easy to operate and require trained personnel (Kurniawan et al., 2006; Saha et al., 2011; Nguyen et al., 2013; Kalidhasan et al., 2016). Adsorption technique on the other hand has shown its potential as a better alternative for the removal of Cr(VI) because it is user friendly, less costly, highly efficient and the adsorbent can be generated (Niu et al., 2019; Zarringhalam et al., 2019; Ou et al., 2020).

In recent years, agricultural waste materials such as rice husk, corn stalk, rice barn and sugarcane bagasse to mention a few, have gained much attention as cheap and readily available adsorbents for the heavy metals remediation. However, these waste materials have been reported to have a poor adsorption capacity toward anion metals. Many researchers have shown that through chemical modification with amine groups their adsorption capacity tends to be enhanced (Chen et al., 2011). For example, Chen et al. (2011), reacted corn stalk with epichlorohydrin and triethylamine using diethylenetriamine as a modifier. Based on the results, the modified corn stalk (MCS) had a point zero charge (pH_{pzc} of 6.5) greater than that of the raw corn stalk (RCS) (pH_{pzc} of 2.9), which suggested that the surface of the MCS contained more positively charged functional groups as compared to RC. The MCS had a better adsorption capacity for Cr(VI) removal even at approximately neutral pH, whereas RC was effective in acid media, at $\text{pH} < 2.9$. In another study reported by Marshall and Wartelle, they quaternized waste materials (i.e., rice hulls, corn stoves and almond shell) with *N*-(3-chloro-2-hydroxypropyl) trimethylammonium chloride (Wartelle and Marshall, 2006). The quaternized waste materials were investigated for the removal of phosphate, arsenate, selenite and chromate from water. The data exhibited that quaternized corn stoves had a good adsorption capacity toward selenite, chromate and arsenate.

In this study, *Moringa Oleifera* was functionalized with amine groups to enhance the adsorption capacity toward Cr(VI) removal. Thereafter, it was reacted with epichlorohydrin and triethylamine in the presence of dimethylformamide (DMF) using diethylamine as a modifier. The iron oxide nanoparticles (Fe_3O_4) were then incorporated in functionalised *Moringa Oleifera* (FMO) to form a magnetic adsorbent ($\text{Fe}_3\text{O}_4/\text{FMO}$). The

advantage of a magnetic adsorbent ($\text{Fe}_3\text{O}_4/\text{FMO}$) is that it can serve as an adsorbent for removal of contaminants from water and it can be removed from aqueous media after the adsorption process using an external magnet, making the recyclability effect of the material possible. Therefore, we report for the first time the removal of this pollutant Cr(VI) using ($\text{Fe}_3\text{O}_4/\text{FMO}$), whereby the *Moringa Oleifera* was first functionalized to enhance the adsorption capacity before the iron oxide nanoparticles were incorporated.

MATERIALS AND METHODS

Materials

All the chemicals used in this study for the synthesis of the adsorbents and batch adsorption studies were of analytical grade. Potassium dichromate (97% purity), Sodium hydroxide pellets (97% purity), Ethanol (99.5%), Methanol (99%), Ammonia solution (35%), Hydrochloric acid (37%), 1,5-Diphenylcarbazide (99% purity), Sulphuric acid (99%), Ferric chloride hexahydrate ($\geq 98\%$ purity), *N,N*-Dimethylformamide (99.8%), Epichlorohydrin (99%), Diethylamine ($\geq 99.5\%$), and Triethylamine ($\geq 99.5\%$) were obtained from Sigma-Aldrich, South Africa.

Preparation of Fe_3O_4 Nanoparticles, FMO, and $\text{Fe}_3\text{O}_4/\text{FMO}$

Fe_3O_4 nanoparticles were synthesized by dissolving 4.05 g $\text{FeCl}_3 \cdot 6\text{H}_2\text{O}$ in 50 mL of deionized water and mixed with 0.5 mL HCl (0.2 M) and ultra-sonicated for 5 min at room temperature. Gradually, 20 mL of 0.3 M NaSO_3 was added to the solution mixture, which resulted in red color. The solution mixture was left for a couple of minutes until the color returned to yellow. Thereafter, the yellow solution was added to 400 mL of deionized water containing 60 mL of 25% ammonia solution and was followed by ultra-sonication for half an hour (30 min). The resultant Fe_3O_4 material was washed with 50/50% ethanol and deionized water (Nejadshafiee and Islami, 2019). The synthesis of functionalized *Moringa Oleifera* was reported in our previous work (Masekela et al., 2020).

For the preparation of a magnetic adsorbent, magnetite was synthesized in the presence of FMO via a co-precipitation method. Here, 4.05 g of Iron Chloride ($\text{FeCl}_3 \cdot 6\text{H}_2\text{O}$) was dissolved in 50 mL of dH_2O and mixed with 0.5 mL of 0.2 M HCl and ultra-sonicated for 5 min at standard temperature. Then 20 mL of 0.3 M NaSO_3 was added to the mixture which resulted in a red color. The solution mixture was left for a couple of minutes until it returned to a yellow color, then 2 g of the functionalized *Moringa Oleifera* (FMO) was poured on to the yellow solution. Thereafter, the yellow solution was added to 400 mL deionised water containing 60 mL of 25% ammonia solution and followed by ultra-sonication for 30 min. The resultant $\text{Fe}_3\text{O}_4/\text{FMO}$ was then washed with 50/50% ethanol and deionised water (Nejadshafiee and Islami, 2019).

Material Characterization

To obtain the physical and chemical properties of the synthesized material ($\text{Fe}_3\text{O}_4/\text{FMO}$) was characterized. Scanning Electron

Microscopy (Zeiss Crossbeam 540, United Kingdom) was used to elucidate the morphology and elemental composition of the adsorbents. For, phase identification, crystallinity and particle size, X-ray diffraction was conducted. The IR spectrum for identification of the functional groups was obtained using the Fourier transform infrared spectroscopy (FTIR, Bruker-Alpha, Germany) at scan range of 500–4,500

cm^{-1} . BET, Micromeritics TriStar II Plus, Germany, was measured to obtain the surface area and pore size of the material. For thermal stability and weight loss determination, a TGA (Hitachi-STA7200RV, Japan) was ran under the nitrogen environment. For surface charge measurements a Zeta potential (Nano ZS-Malvern, United Kingdom) was used.

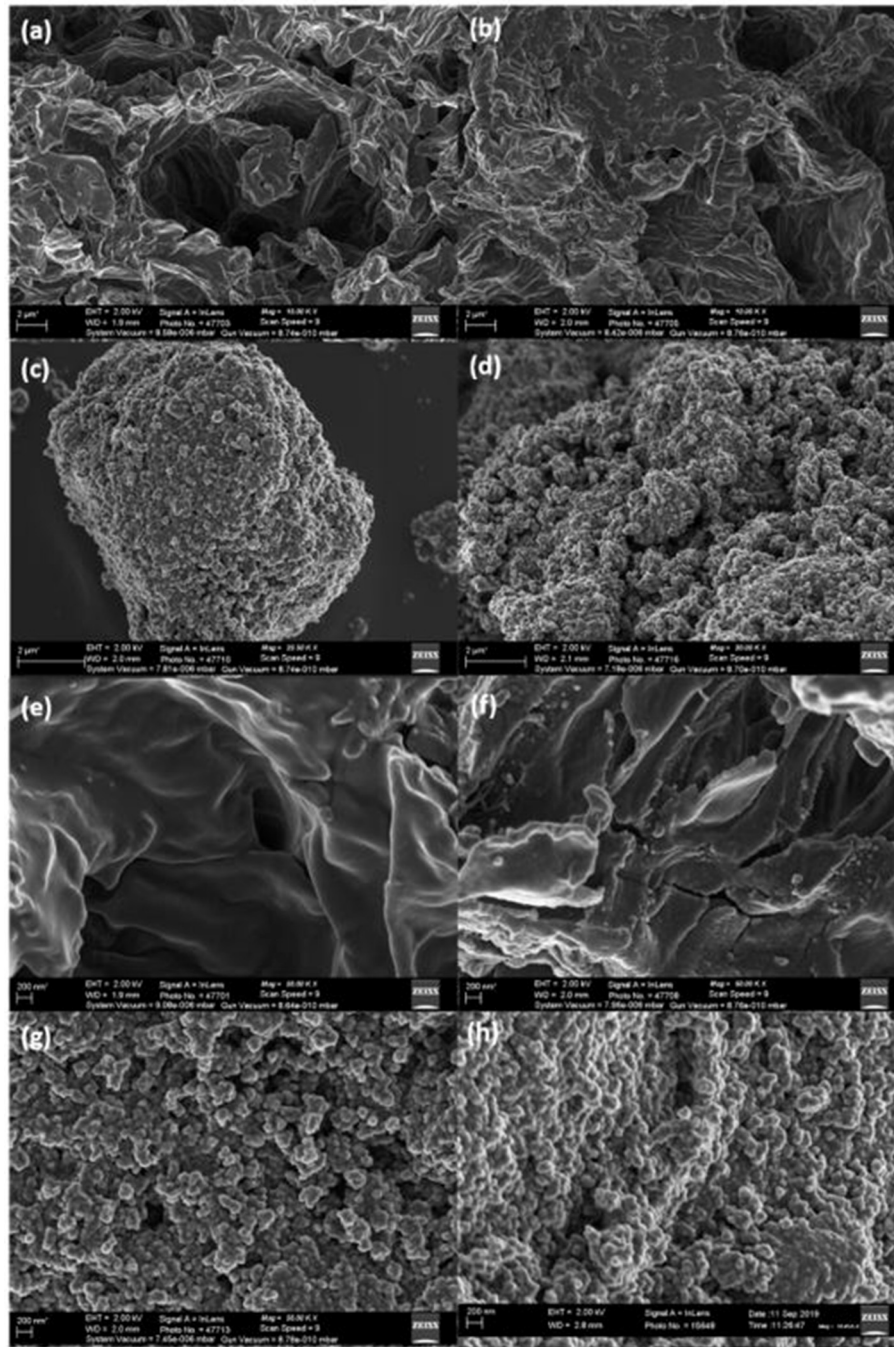


FIGURE 1 | FE-SEM images of (a) MO, (b) FMO, (c) Fe₃O₄ and (d) Fe₃O₄/FMO at 2 μm (e) MO (f) FMO (g) Fe₃O₄ and (h) Fe₃O₄/FMO at 200 nm.

Batch Adsorption Studies

To obtain optimum parameters for the removal of the pollutant, using the batch method, parameters such as dosage, pH, uptake time and concentration were investigated. The pH effect at various values (2–10) was used to investigate whether Cr(VI) removal by $\text{Fe}_3\text{O}_4/\text{FMO}$ depends on the pH and also to determine the optimum removal pH. In this experiment, a known amount of $\text{Fe}_3\text{O}_4/\text{FMO}$ was dispersed into 100 mL of reagent bottle with 50 mL of pollutant concentration. The reagent bottles were taken into a shaker water bath and agitated at 200 rpm speed for 24 hrs with a fixed temperature of 25°C in all experiments. To obtain the optimum dosage to be used, different amounts of the adsorbents were varied from 0.05 to 0.4 g with 100 mg/L Cr(VI) concentration fixed and at optimum pH 2. Lastly, the adsorption studies on the effect of time were conducted at different time intervals (5–140 min) until equilibrium was reached.

Cr(VI) Detection Using UV-Vis Spectrophotometry

In this study UV-vis spectrophotometry (Agilent Technologies Cary 60 UV-Vis, Malaysia) was used for the detection of Cr(VI) at 540 nm wavelength using colorimetric method (1,5-Diphenylcarbazide) (Yusof and Malek, 2009).

For the preparation of Diphenylcarbazide (DPC) solution, an amount of 0.125 g (1.5 Diphenylcarbazide) was dissolved into 25 mL of 99.8% methanol. The solution mixture was added into 132 mL of H_2SO_4 (5.2%) using 250 mL volumetric flask. Thereafter, the solution was diluted with deionized water until 250 mL mark. For Cr(VI) detection, the DPC solution was mixed with Cr(VI) sample to form a DPC to Cr(VI) ratio 1:3. The mixture solution turned into violet colored complex whose absorbance wavelength was measured to be 520 nm using UV-vis spectrophotometry (Agilent Technologies Cary 60 UV-Vis, Malaysia).

RESULTS AND DISCUSSIONS

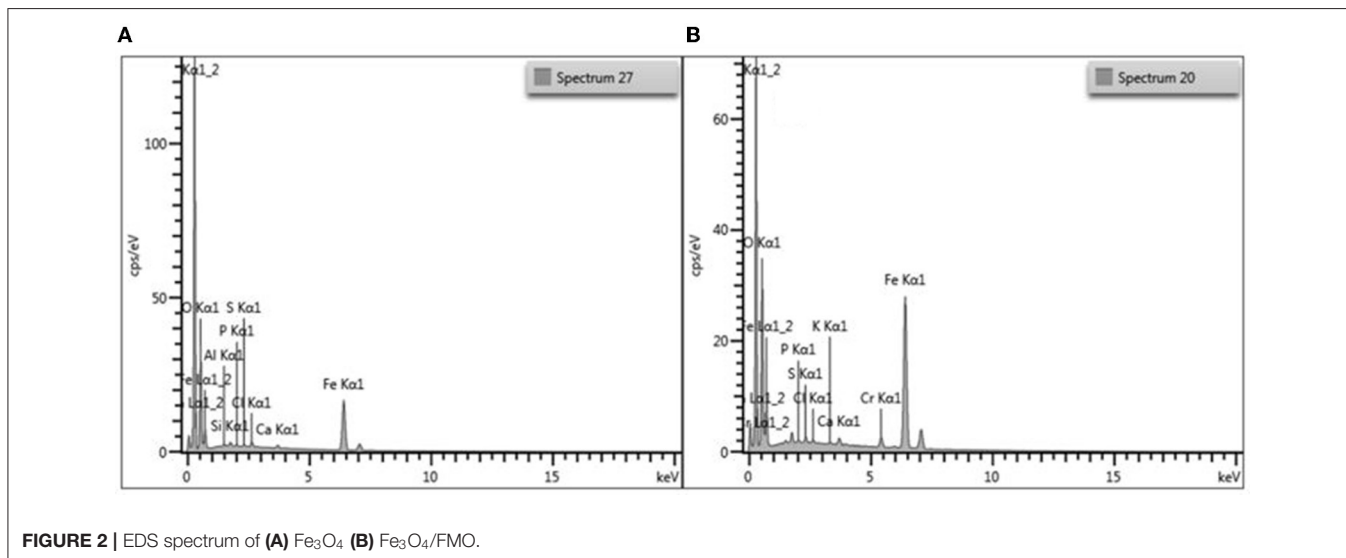
Morphological Analysis

FESEM (Figures 1a–h), was conducted to study the surface morphology of the adsorbents (MO, FMO, Fe_3O_4 , and $\text{Fe}_3\text{O}_4/\text{FMO}$) at different magnifications (low and high). In Figures 1a,b, the surface morphology of MO had some irregular flake shape and pores, while for FMO the external surface appeared to be rough after chemical modification. In Figures 1c,d, the magnetite nanoparticles appeared to be spherical in shape covering the external surface of FMO, while the spherical nanoparticles on the surface of FMO appeared to be agglomerated as well. At higher magnifications (Figures 1e–h), it is clearly visible that the external surface of the MO flakes were smooth with less pores before any modifications, however after chemical functionalization with amine groups, the FMO showed increase in number of openings (pores) which confirmed their improved adsorption capability toward Cr(VI) from our previous studies (Masekela et al., 2020).

Furthermore, the presence of Fe element in the EDS spectrum of the composite showed an evident successful incorporation iron nanoparticles on the surface of FMO (Figure 2A). Before adsorption, no chromium element peak was detected in the EDS spectrum, however after adsorption new peaks which corresponded to chromium were detected, thus confirming adsorption of Cr(VI) by magnetic adsorbent (Figure 2B). To further confirm the formation of these materials, identification of the groups present [grafting of the amine functional groups onto *Moringa Oliefera* (MO)] and incorporation of the Fe_3O_4 on the FMO, FTIR analysis was conducted.

Functional Group and Formation Analysis

Figure 3 presents the Infrared (IR) spectra of MO, FMO, Fe_3O_4 and $\text{Fe}_3\text{O}_4/\text{FMO}$. The IR spectra for FMO displayed peaks at $1,647$ and $1,030\text{ cm}^{-1}$ which can be attributed to N-H stretching band of amino groups, while the broad band at $3,369$ – $3,299$, $1,351$, $1,621$, and $1,020$ were ascribed to –OH



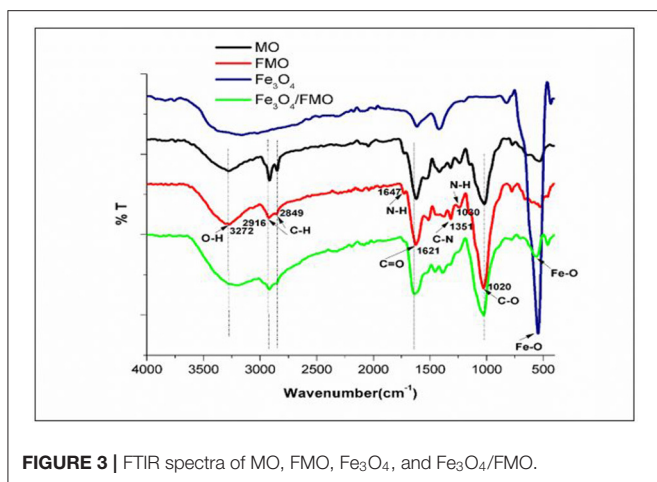


FIGURE 3 | FTIR spectra of MO, FMO, Fe_3O_4 , and $\text{Fe}_3\text{O}_4/\text{FMO}$.

or $-\text{NH}$, $\text{C}-\text{N}$, $\text{C}=\text{O}$ and $\text{C}-\text{O}$ groups, respectively. The IR spectra of magnetite (Fe_3O_4) indicated a very sharp intense peak at the fingerprint region (685 cm^{-1}) attributed to $\text{Fe}-\text{O}$ vibration (Niu et al., 2019). It can be observed that the absorption bands for FMO were preserved within the composites after the successful incorporation of magnetite nanoparticles. Therefore, the incorporation of magnetite did not destroy FMO structure.

Structural, Surface Area, and Thermal Stability Studies

Further confirmation of crystallinity, structural and phase analysis, XRD was applied to MO, FMO, Fe_3O_4 and $\text{Fe}_3\text{O}_4/\text{FMO}$ (Figure 4A). The XRD patterns for MO and FMO showed that these materials are amorphous in nature. The introduction of iron oxide (Fe_3O_4) onto FMO resulted in crystallinity of the composite. The XRD diffraction peaks at 2θ values of 30.21 , 35.53 , 43.31 , 54.50 , 57.30 , 62.90 , and 74.3° corresponded to miller index (220), (311), (400), (422), (511), (440), and (533), respectively, which are representative of the iron oxide formation (Chen et al., 2012; Ding et al., 2015). It was observed that there was a broad carbon peak at 2θ value 20° with the miller index (002) for FMO on the composite.

The surface area and pore sizes of the MO, FMO, Fe_3O_4 , and $\text{Fe}_3\text{O}_4/\text{FMO}$ were measured using the BET surface analyzer. The MO surface area was $1.9198\text{ m}^2/\text{g}$. Upon the successful introduction of amine groups onto MO, a lower surface area to $1.0942\text{ m}^2/\text{g}$ was observed. The incorporation of magnetite onto FMO surface resulted in a huge increase in surface area from 1.0942 to $30.6387\text{ m}^2/\text{g}$. This might be due to a high amount of magnetic particle dispersion on the FMO surface, which has a particular high surface area ($52.2834\text{ m}^2/\text{g}$) (Popoola, 2019). Similar studies were reported in the literature (Hu et al., 2011; Panneerselvam et al., 2011; Zainol et al., 2015), where magnetic impregnation increases the BET surface area of the parent materials. The average pore size of FMO also increased from 13.770 to 25.0386 nm upon successful incorporation of magnetite nanoparticles and also indicated that these materials were mesoporous in nature.

Figures 4B,C display the nitrogen adsorption-desorption isotherms of the prepared materials (MO, FMO, Fe_3O_4 , and $\text{Fe}_3\text{O}_4/\text{FMO}$). According to the International Union of Pure and Applied Chemistry (IUPAC), MO, and FMO were classified as type II, whereas Fe_3O_4 and $\text{Fe}_3\text{O}_4/\text{FMO}$ as type III from the hysteresis loops. To further understand the characteristic nature of these materials and their stability, thermal gravimetric analysis was employed.

TGA was also conducted to determine the thermal stabilities of MO, FMO, Fe_3O_4 , and $\text{Fe}_3\text{O}_4/\text{FMO}$ in Figure 4D. The TGA analysis for MO and FMO showed that both adsorbents started to decompose at 210 until 350°C and could be due to the dehydroxylation of MO and structural decomposition of FMO. These results were corroborated by other studies as reported by Araújo et al. (2010), whereby *Moringa Oleifera* seeds started to decompose at $\sim 200^\circ\text{C}$. The magnetite (Fe_3O_4) illustrated that it was more thermally stable compared MO and FMO. The TGA curve of $\text{Fe}_3\text{O}_4/\text{FMO}$ behaved in a similar manner to the parent material (FMO). However, the incorporation of magnetite onto FMO enhanced the thermal stability of the composites since it was noticed that weight loss for $\text{Fe}_3\text{O}_4/\text{FMO}$ was minimized. The enhancement of the thermal stability also confirmed successful incorporation of magnetite nanoparticles onto FMO. The magnetic adsorbent ($\text{Fe}_3\text{O}_4/\text{FMO}$) was the most thermally stable material compared to parent materials (MO and FMO), its weight loss was $\sim 40.65\%$ above 650°C . The weight loss for MO and FMO (parent materials) above 650°C were found to be more than 68 and 99%, respectively (Figure 4D).

The DTG analysis was also conducted, for MO and FMO, a huge endothermic peak at $\sim 350^\circ\text{C}$ was identified in Figure 4E. These peaks indicated thermal decomposition of both adsorbents. The DTG curve of $\text{Fe}_3\text{O}_4/\text{FMO}$ displayed two distinctive endothermic peaks at ~ 300 and 450°C , which confirmed the weight losses related to decomposition of the composites. These results corroborate with the TGA data in Figure 4D.

Surface Charge Studies

The surface charge of the prepared adsorbents (MO, FMO, and $\text{Fe}_3\text{O}_4/\text{FMO}$) were measured using Zetasizer Nano ZS-Malvern. As shown in Figure 5, the point of zero charges of the materials were measured at different pH values of the solutions (2–10). It can be observed that after chemical modification of MO with amine groups the pH zero point charge increased from 2.0 to 4.0, suggesting that FMO contained more positively charged functional groups compared to MO. This is an advantage because in aqueous solutions, Cr(VI) exist in the form of anions ($\text{Cr}_2\text{O}_7^{2-}$, HCrO_4^- , and $\text{Cr}_2\text{O}_7^{2-}$). Upon a successfully incorporation of magnetite onto FMO, the pH zero point (pH_{zpc}) increased from 4.0 to 5.0. The obtained point of zero charge (pH_{zpc}) was higher than that of modified activated carbon (Huang et al., 2009), coffee husk (Oliveira et al., 2008), oxidized corn hob (Leyva-Ramos et al., 2005) and thuja orientalis (Malkoc, 2006).

As depicted in Figure 5, the maximum pollutant [Cr(VI)] removal was observed at $\text{pH} < 5$ due to the attraction of positively charged adsorbents and negatively charged ions of Cr(VI) in the form of $\text{Cr}_2\text{O}_7^{2-}$ and HCrO_4^- .

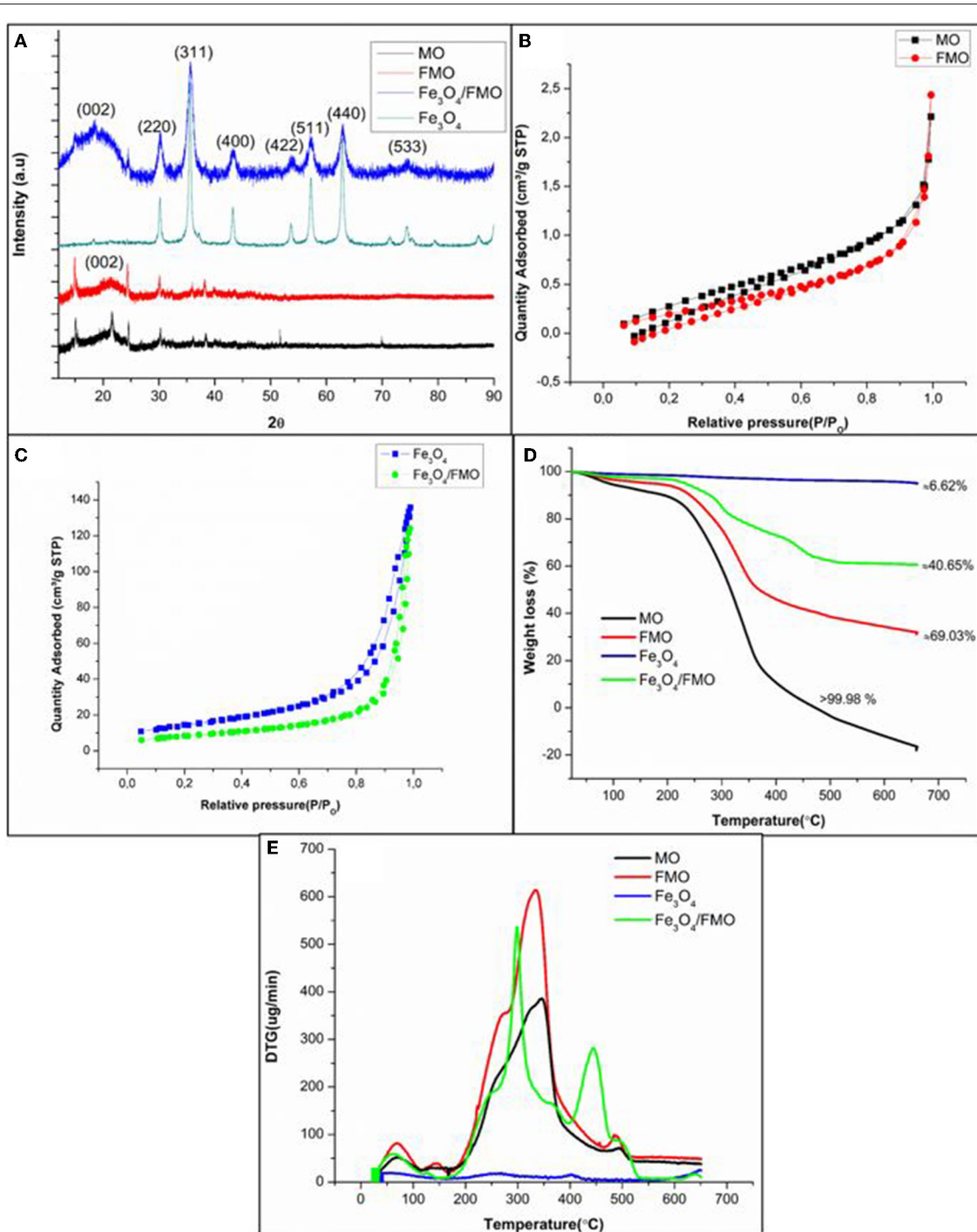


FIGURE 4 | Characterization of MO, FMO, Fe₃O₄, and Fe₃O₄/FMO using (A) XRD (B,C) Nitrogen adsorption/desorption isotherms (D) TGA curves and (E) DTG curves.

Batch Adsorption Studies

Influence of pH, Dosage, Contact Time, and Concentration for Cr(VI) Uptake

The pH is known to play a pivotal role in the adsorption ability and stability of the suspended catalyst. The effect of pH on Cr(VI) removal is presented in **Figure 6A**. This experiment was

conducted to investigate whether the removal of the pollutant is dependent on the pH. As noted, at low pH (2) regions about 90.1% of Cr(VI) was removed, furthermore as the pH increased the removal ability was decreased till 25% at pH 10. The reason for this high Cr(VI) removal at low pH could be caused by the surface of the adsorbent being protonated hence making

the adsorbent surface positively charged. Thus, the positively charged adsorbents interacted with Cr(VI) oxy anions ($\text{Cr}_2\text{O}_7^{2-}$ and HCrO_4^-) via electrostatic interaction (Timbo et al., 2017).

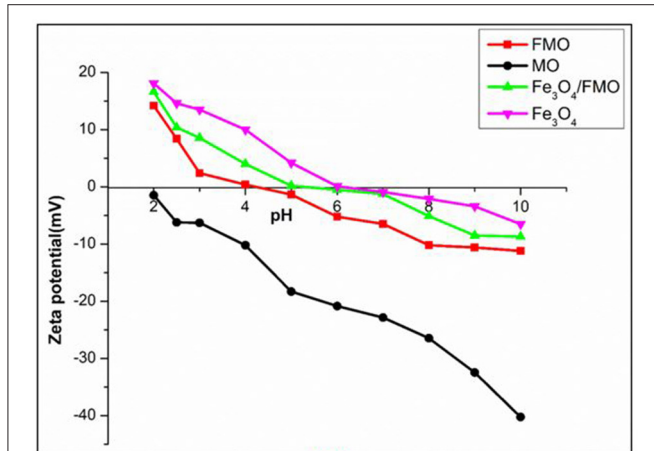


FIGURE 5 | Determination of the surface charge of MO, FMO, Fe_3O_4 , and $\text{Fe}_3\text{O}_4/\text{FMO}$ using the Zeta potential.

The effect of $\text{Fe}_3\text{O}_4/\text{FMO}$ dosage on the removal of Cr(VI) was investigated. **Figure 6B** displayed Cr(VI) removal percentage with respect to different amounts of magnetic functionalized *Moringa Oleifera* ($\text{Fe}_3\text{O}_4/\text{FMO}$). From **Figure 6B** the amount of the pollutant removed with a higher $\text{Fe}_3\text{O}_4/\text{FMO}$ dosage amount is presented. At 0.15 g of $\text{Fe}_3\text{O}_4/\text{FMO}$, a maximum amount of 94% of Cr(VI) was removed. As can be depicted we can stipulate that, a higher dosage resulted in more active sites, until the saturation or equilibrium point was reached. In similar studies that had been done previously using *Moringa Oleifera*, Shirani et al. (2018), used 2.5 g of raw *Moringa Oleifera* pods powder (MPP) with a removal efficiency of about 82%. In this study though, a far less amount was used with a better removal of 94%. This indicates that the functionalization and incorporation of the magnetite in FMO was very effective. Also, it was important to check the effect of the dosage as too much of the catalyst usage needs to be avoided as excess use might later cause agglomeration. Furthermore, for recovery studies, due to the magnetic effect this material has, it can easily be recovered when used in wastewater systems as indicated by the inserted picture in **Figure 6B**.

To examine the optimum time needed for the removal of Cr(VI), adsorption studies of Cr(VI) on magnetic functionalized

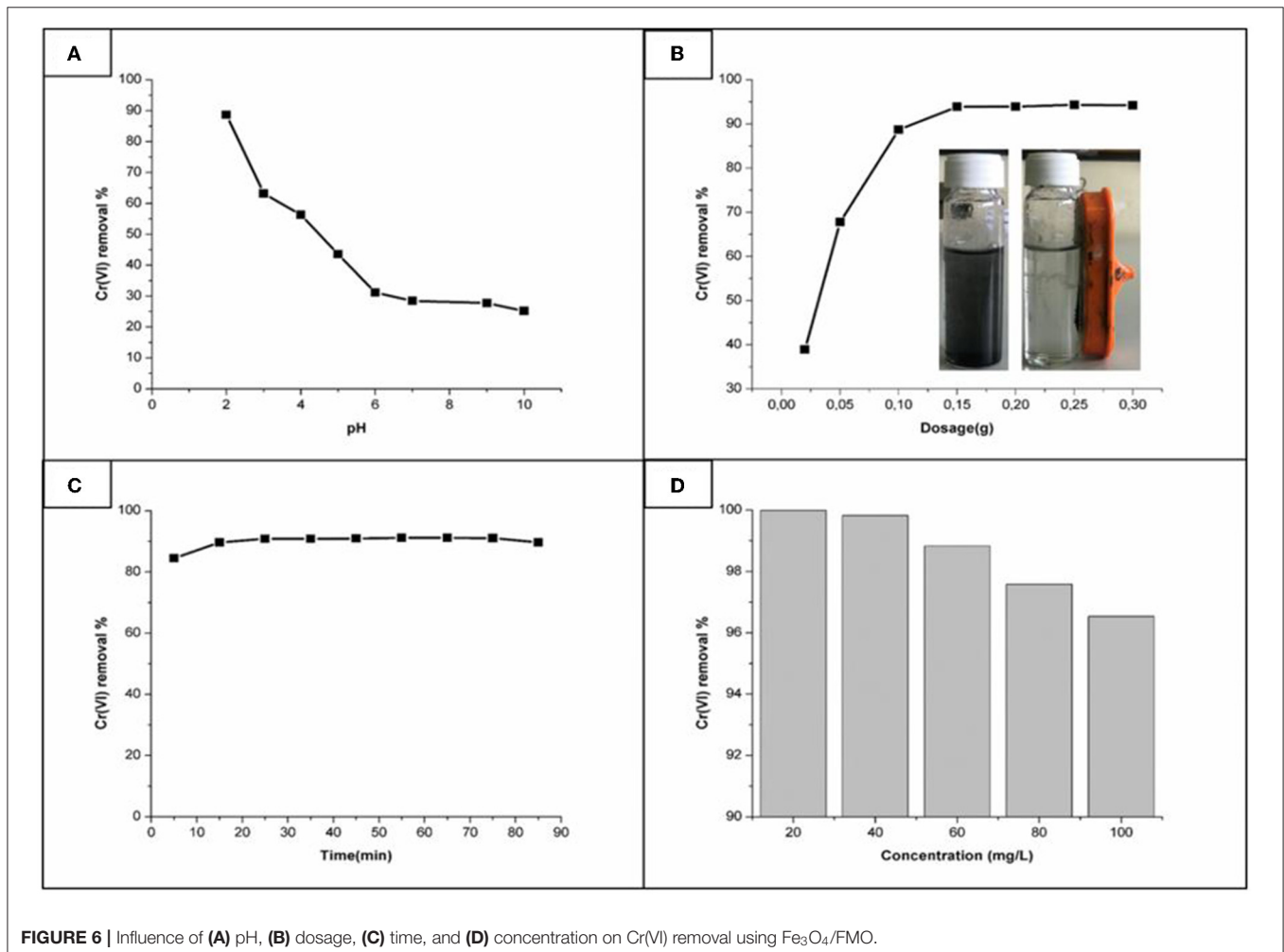


FIGURE 6 | Influence of (A) pH, (B) dosage, (C) time, and (D) concentration on Cr(VI) removal using $\text{Fe}_3\text{O}_4/\text{FMO}$.

Moringa oleifera ($\text{Fe}_3\text{O}_4/\text{FMO}$) was conducted at different time intervals (from 5 until 90 min). **Figure 6C** displayed the effect of time for the removal of Cr(VI) using $\text{Fe}_3\text{O}_4/\text{FMO}$ as an adsorbent. It was noted that the adsorption equilibrium was attained at 25 min, which was a far less time as reported in previous studies. According to the study conducted by Sasikala and Muthuraman (2015) using raw *Moringa Oleifera*, the adsorption equilibrium was reported after 2 h (120 min). Noticeably, the removal efficiency after 25 min was not reduced, even till 90 min but a plateau was reached. It could suggest during the experiment, the catalyst did not reach a stage of inactivation (Oliveira et al., 2008).

The experimental studies for the effect of initial concentration using magnetic adsorbent were conducted using different solutions containing 20–100 mg/L of Cr(VI) with optimum conditions (pH 2, dose of 0.15 g $\text{Fe}_3\text{O}_4/\text{FMO}$ and contact time of 25 min), **Figure 6D**. From the results it is clear that increasing dosage amount did not result in a higher removal ability, instead the inverse occurred, whereby less pollutant removal was observed. This could be due to the catalyst saturation occurring within thus blocking the available adsorption sites. Similar behavior was observed when using raw *Moringa Oleifera* (MO) (Timbo et al., 2017). It can be noted that 20 mg/L of $\text{Fe}_3\text{O}_4/\text{FMO}$ completely removed Cr(VI) from solution. Though there was a decrease at higher concentrations it is worth noting that even at 100 mg/L the pollutant removal was still more than 95% which demonstrated the efficiency of this material.

Adsorption Kinetics

The adsorption mechanism of Cr(VI) was determined using two kinetic models, pseudo-first and pseudo-second order models.

Pseudo-First-Order

The early stages of adsorption processes are often represented by this model. The linear Equation (1) (Huang, 2019) is shown

below to describe this model.

$$\ln(q_e - q_t) = \ln q_e - k_1 t \quad (1)$$

q_e (mg/g) represents the amount of Cr(VI) adsorbed on the adsorbent, q_t (mg/g) is the adsorbed Cr(VI) amount on the adsorbent at a certain times (t), and k_1 is known as the 1st order constant. Parameters such as k_1 , q_e and q_t will be calculated using the linear plot obtained from Equation (1).

Pseudo-Second-Order

This model works on the assumption that the interaction between the pollutant and adsorbent at the surface maybe chemisorption. Chemisorption involves the interaction of the metal ions (pollutant) and adsorbent via chemical bonding (Wan et al., 2010). The linear Equation (2) for 2nd order model is represented below as

$$\frac{t}{q_t} = \frac{1}{k_2 q_e^2} + \frac{1}{q_e} t \quad (2)$$

k_2 (g/mg min) represents the 2nd order rate constant. At equilibrium, q_e represents the adsorbed amount of the pollutant q_t at certain times (q_t), as these are generally obtained from the linear plot graph in **Figures 7A,B** and presented in **Table 1**. The correlation coefficient (R^2) determines which model will fit with experimental data. The experimental data showed that pseudo 2nd order was more favorable compared to the 1st order mechanism, since its correlation coefficient value was greater than ($R^2 = 0.99999$) whereas to pseudo 1st order model ($R^2 = 0.53454$) was lower. This suggested that the adsorption mechanism between Cr(VI) and $\text{Fe}_3\text{O}_4/\text{FMO}$ was through chemical interaction (chemisorption) (Contreras et al., 2007; Wang et al., 2015; Gorzin and Bahri Rasht Abadi, 2018; Liu et al., 2019; Murcia-Salvador et al., 2019).

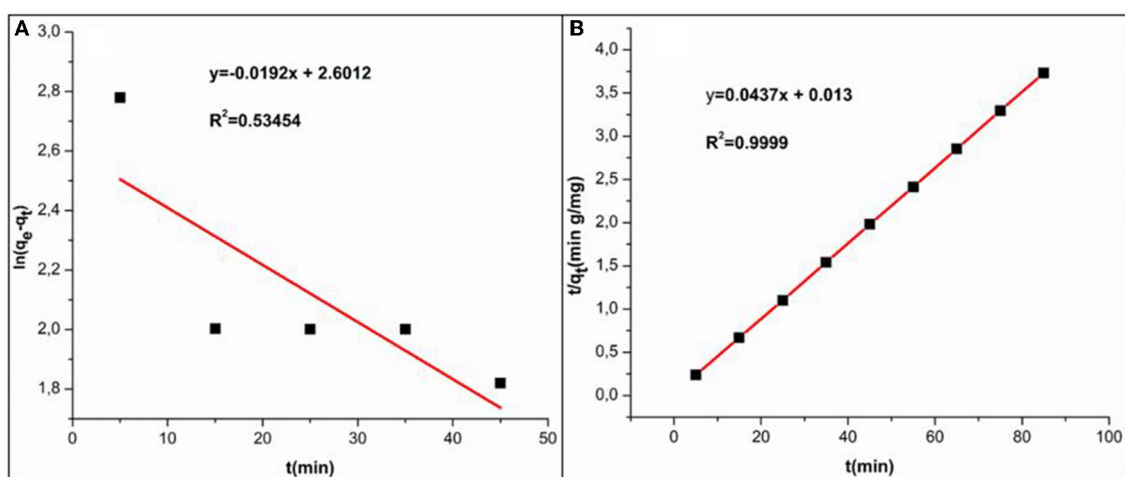


FIGURE 7 | (A) Linear Pseudo-first-order; **(B)** Pseudo-second-order model for Cr(VI) adsorption by $\text{Fe}_3\text{O}_4/\text{FMO}$.

Adsorption Isotherms

Adsorption isotherms are important tools to describe the nature of interaction between adsorbent and adsorbate. In this study, two known isotherms models namely Freundlich and Langmuir isotherm models were used to fit the adsorption experimental data obtained for Cr(VI).

Freundlich Isotherms

Freundlich adsorption isotherm model is an empirical model for describing adsorption by heterogeneous surfaces (adsorbent) beyond the first monolayer. It further assumes that stronger available binding sites on the surfaces are firstly occupied, and that adsorption further increases as more available adsorption binding sites increases (Duranoglu et al., 2012). The Freundlich adsorption isotherm model is mathematically expressed as shown by linear Equation (3) below.

$$\ln q_e = \ln K_F - \frac{1}{n} \ln C_e \quad (3)$$

Whereby K_F and $1/n$ are linked to adsorption capacity and dimensionless heterogeneity factor, respectively. The linear plot of $\ln q_e$ vs. $\ln C_e$ that demonstrates the validity of Freundlich adsorption isotherm model is shown in **Figure 8A**.

Langmuir Isotherms

The Langmuir model implies that adsorption energies on the adsorbent's surface are uniform, that adsorbate ions do not transigrate in the plane of the surface, and that the adsorbent's surface is homogenous (Hamdaoui and Naffrechoux, 2007). It also implies that when the monolayer has been covered, no additional adsorption occurs (Dada et al., 2012). The Langmuir equation is expressed in linear form as follows:

$$\frac{C_e}{q_e} = \frac{1}{k_L q_m} + \frac{C_e}{q_m} \quad (4)$$

Where q_m (mg/g) and k_L (L/mg) represent maximum adsorption capacity and Langmuir constant linked to adsorption energy, respectively. C_e is the equilibrium concentration, and q_e is the equilibrium adsorption capacity. A linear plot of C_e/q_e vs. C_e obtained from experimental data of Cr(VI) adsorption is shown in **Figure 8B**.

The Freundlich and Langmuir adsorption isotherms parameters obtained from linear plots in **Figure 8** were presented in **Table 2**. The correlation coefficient (R^2) obtained from Langmuir linear plot was higher as compared to Freundlich isotherm, thus indicating that Cr(VI) adsorption by Fe_3O_4/FMO followed monolayer adsorption.

The dimensionless separation factor (R_L) is an essential characteristic of the Langmuir isotherms to determine

TABLE 1 | Data for Pseudo first order and Pseudo second order.

Pseudo first order		Pseudo second order	
Linear		Linear	
q_e	13.480	q_e	22.883
K_1	0.0192	K_2	0.147
R^2	0.53454	R^2	0.99999

TABLE 2 | Data for Freundlich and Langmuir isotherms.

Freundlich isotherms		Langmuir isotherms	
Linear		Linear	
K_F	0.508	q_m	0.735
$1/n$	0.27719	k_L	4.202
R^2	0.94667	R^2	0.97089

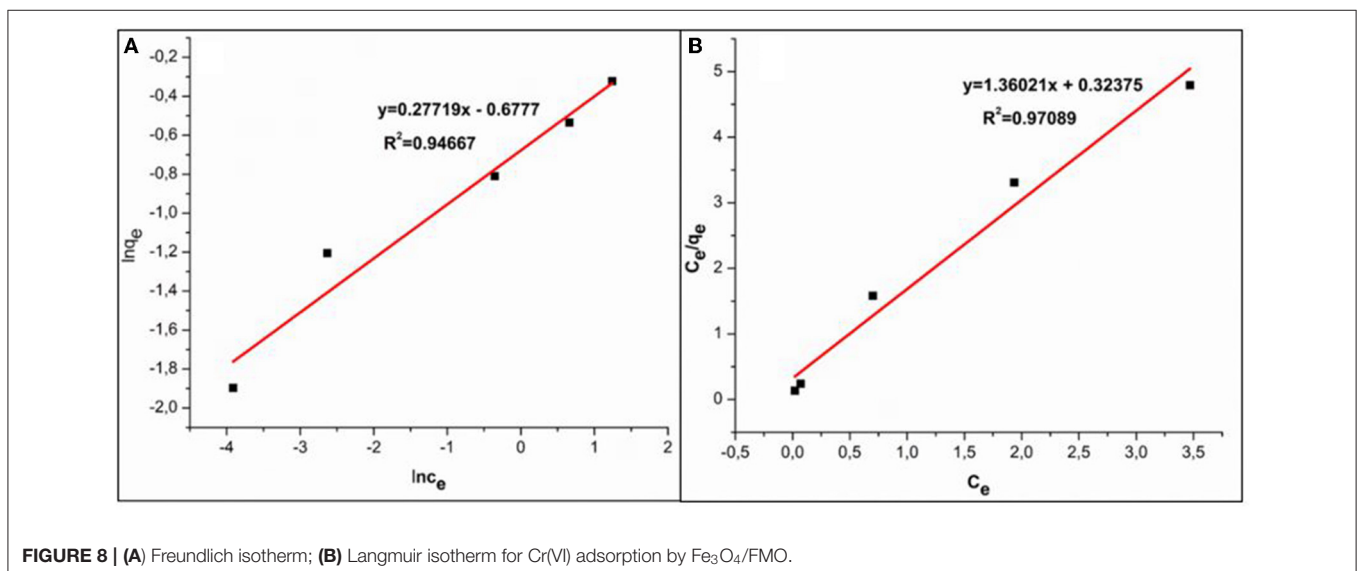
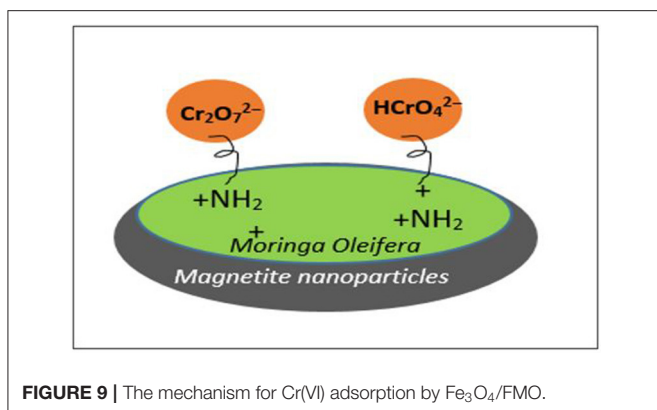


FIGURE 8 | (A) Freundlich isotherm; (B) Langmuir isotherm for Cr(VI) adsorption by Fe_3O_4/FMO .



favourability of the adsorption, and it is expressed as (Peng et al., 2018):

$$R_L = \frac{1}{1 + k_L C_0} \quad (5)$$

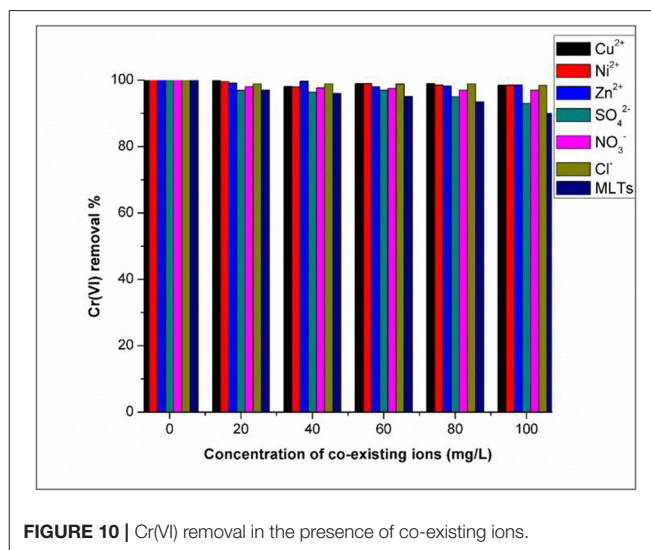
Where k_L and C_0 represent Langmuir constant and highest concentration of Cr(VI), respectively. The R_L value indicates if the Langmuir isotherms is either favorable ($0 < R_L < 1$), unfavorable ($R_L > 1$), irreversible ($R_L = 0$), and linear ($R_L = 1$). In this study, the experimental R_L value was calculated to be 0.002 for Cr(VI) adsorption, thus indicating that Langmuir isotherm was favorable for Cr(VI) adsorption by Fe₃O₄/FMO.

Mechanism of Adsorption

The Cr(VI) anions exist as HCrO_4^{2-} and $\text{Cr}_2\text{O}_7^{2-}$ at pH 2 and 6, in aqueous solution. These anionic Cr(VI) species are adsorbed by protonated functional groups of the adsorbent as depicted in **Figure 5**. At pH above 6, there is no significant Cr(VI) adsorption since HCrO_4^{2-} and $\text{Cr}_2\text{O}_7^{2-}$ tend to compete with OH^- for available active adsorption sites. Therefore, the possible mechanism of Cr(VI) onto Fe₃O₄/FMO could be associated with electrostatic interaction between protonated adsorbent (positively charged adsorbent) with Cr(VI) anionic species (i.e., HCrO_4^{2-}) at acidic media. Furthermore, the adsorption mechanism was based on a chemisorption interaction. This was also confirmed by the pseudo second order in **Figure 7** and the data in **Table 1**. Hence the mechanism in **Figure 9** is proposed for this study.

The Influence of Co-existing Ions on the Removal of Cr(VI) by Fe₃O₄/FMO

This experiment was conducted to investigate the selectivity of magnetic functionalized *Moringa Oleifera* (Fe₃O₄/FMO) toward Cr(VI) removal in the presence of cations and anions. For this study, a few selected ions at various concentrations (Zn^{2+} , Cu^{2+} , Ni^{2+} , NiO_3^- , SO_4^{2-} , and Cl^-) were studied for their influence on the removal the pollutant as displayed in **Figure 10**. From the data it is clear that the presence of cations in the solution did not have an effect on the removal of Cr(VI) which suggested the synthesized Fe₃O₄/FMO was selective toward Cr(VI) in the presence of cations. As depicted in **Figure 5**, the surface



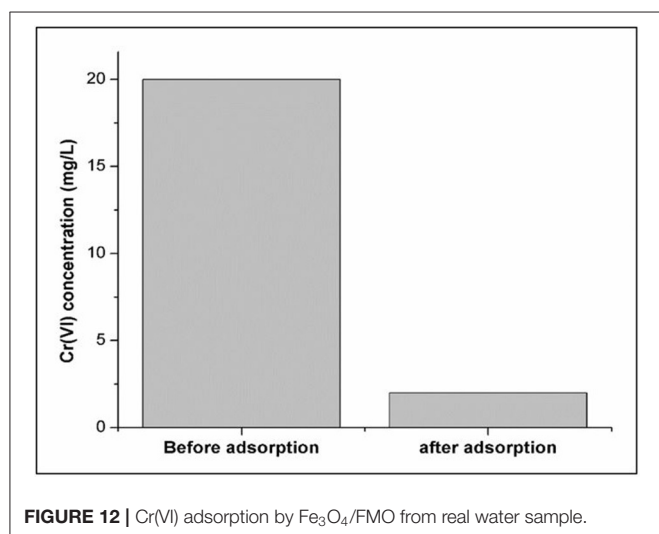
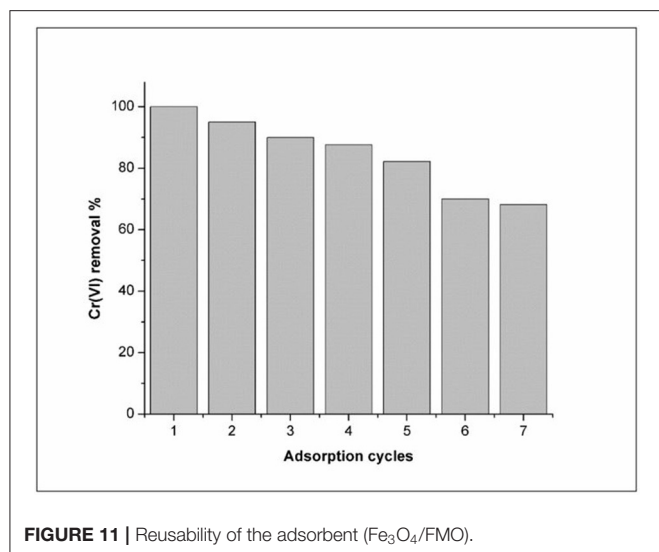
of Fe₃O₄/FMO was positively charged which therefore made it impossible to attract positively charged ions (metal cations) via electrostatic interaction. In the presence of anions there was an effect though it was minimal in particular for NiO_3^- and Cl^- as depicted in **Figure 10**. In the case of SO_4^{2-} in particular at high concentrations, the removal of Cr(VI) was significantly reduced since the percentage removal decreased from 99 to 93.02%. This effect could be due to similar structure between Cr(VI) molecules and SO_4^{2-} which resulted in the competition for adsorption sites on the surface of Fe₃O₄/FMO (Eskandarpour et al., 2008).

Reusability Studies

To ensure we are able to produce cost effective materials, it is important to test how many times a material can be reused. The Fe₃O₄/FMO adsorbent for Cr(VI) removal, adsorption studies were conducted for several number of cycles (7). **Figure 11** illustrated the sorption efficiency of the regenerated adsorbent (Fe₃O₄/FMO) after 7 adsorption cycles. The removal efficiency of the adsorbent was reduced upon an increase in adsorption cycles. This could be caused by the loss of stability of the adsorbent after regeneration after several adsorption cycles (Bhaumik et al., 2012). As it can be noticed from **Figure 9**, the Cr(VI) removal was slightly reduced even after the 1st cycle, as the amount removed reduced drastically. From the 4th cycle onwards, the removal efficiency dramatically decreased from 87.64 to 68.2%.

Real Water Analysis

In **Figure 12**, the adsorption of Cr(VI) spiked real water sample using magnetic functionalized *Moringa Oleifera* (Fe₃O₄/FMO) under optimized conditions is displayed. It can be observed that the initial concentration of Cr(VI) was 20 mg/L and after adsorption the pollutant was reduced to 2 mg/L. Therefore, this meant that Fe₃O₄/FMO removed 90% of the pollutant from the real water sample. The limit of detection (LOD) and quantification (LOQ) obtained from the linear calibration curve of Cr(VI) were 0.1486 and 0.446 mg/L, respectively.



CONCLUSIONS

In this study, Fe₃O₄ was successfully incorporated onto FMO to obtain a magnetic adsorbent that can be recovered from the sample after application. The modification of Fe₃O₄/FMO was confirmed by XRD, FTIR, and SEM analysis. The highest Cr(VI) removal percentage by Fe₃O₄/FMO was above 90%

REFERENCES

- Araújo, C. S., Alves, V. N., Rezende, H. C., Almeida, I. L., De Assuncao, R., Tarley, C. R., et al. (2010). Characterization and use of *Moringa oleifera* seeds as biosorbent for removing metal ions from aqueous effluents. *Water Sci. Technol.* 62, 2198–2203. doi: 10.2166/wst.2010.419
- Bhaumik, M., Maity, A., Srinivasu, V. V., and Onyango, M. S. (2012). Removal of hexavalent chromium from aqueous solution using polypyrrole-polyaniline nanofibers. *Chem. Eng. J.* 181, 323–333. doi: 10.1016/j.cej.2011.11.088

and it was obtained at a low pH (2). The chemisorption interaction between Cr(VI) and Magnetic adsorbent was established and it was confirmed by pseudo 2nd order and adsorption kinetics.

Reusability studies displayed that the material may be applied for 4 cycles and the removal percentage remained above 90%. The adsorbent (Fe₃O₄/FMO) was highly selective toward Cr(VI) in the presence of other cations. The applied adsorbent (Fe₃O₄/FMO) was easily separated from aqueous solution due to the magnetic Fe₃O₄ nanoparticles. Therefore, this adsorbent has a potential of being applied in industrial wastewater treatment to simultaneously remove the adsorbent and the adsorbent contaminant from wastewater.

DATA AVAILABILITY STATEMENT

The raw data supporting the conclusions of this article will be made available by the authors, without undue reservation.

AUTHOR CONTRIBUTIONS

DM: data curation, formal writing, and editing. TY: formal writing and editing. NH-M and NM: supervision, editing and resources. All authors contributed to the article and approved the submitted version.

FUNDING

This work was supported by the Centre of Nanomaterials Science Research—purchasing chemicals, National Research Foundation—student bursary and publications, and University of Johannesburg—publications, books and other research related costs.

ACKNOWLEDGMENTS

The authors would like to thank the contribution of the following funders, National Nanoscience Postgraduate Teaching and Training Platform (NNPTTP, grant no. 0036/2019), Department of Science and Innovation (DSI), Centre of Nanomaterials Science Research, NRF Thuthuka (grant no. 107066), and the Faculty of Science at the University of Johannesburg (UJ). The University of Limpopo (chemistry department) and NRF Thuthuka (UID117999) is also acknowledged for their financial support.

- Chen, D., Li, Y., Zhang, J., Zhou, J. Z., Guo, Y., and Liu, H. (2012). Magnetic Fe₃O₄/ZnCr-layered double hydroxide composite with enhanced adsorption and photocatalytic activity. *Chem. Eng. J.* 185, 120–126. doi: 10.1016/j.cej.2012.01.059
- Chen, S., Yue, Q., Gao, B., Li, Q., and Xu, X. (2011). Removal of Cr(VI) from aqueous solution using modified corn stalks: characteristic, equilibrium, kinetic and thermodynamic study. *Chem. Eng. J.* 168, 909–917. doi: 10.1016/j.cej.2011.01.063
- Cieślak-Golonka, M. (1996). Toxic and mutagenic effects of chromium (VI). A review. *Polyhedron* 15, 3667–3689. doi: 10.1016/0277-5387(96)00141-6

- Contreras, E. G., Martinez, B. E., Sepúlveda, L. A., and Palma, C. L. (2007). Kinetics of basic dye adsorption onto sphagnum magellanicum peat. *Adsorp. Sci. Technol.* 25, 637–646. doi: 10.1260/026361707785082396
- Dada, A. O., Olalekan, A. P., Olatunya, A. M., and Dada, O. J. I. C. (2012). Langmuir, Freundlich, Temkin and Dubinin–Radushkevich isotherms studies of equilibrium sorption of Zn²⁺ onto phosphoric acid modified rice husk. *IOSR J. Appl. Chem.* 3, 38–45. doi: 10.9790/5736-0313845
- Ding, C., Cheng, W., Sun, Y., and Wang, X. (2015). Novel fungus-Fe₃O₄ bio-nanocomposites as high performance adsorbents for the removal of radionuclides. *J. Hazard. Mater.* 295, 127–137. doi: 10.1016/j.jhazmat.2015.04.032
- Duranoglu, D., Trochimczuk, A. W., and Beker, U. (2012). Kinetics and thermodynamics of hexavalent chromium adsorption onto activated carbon derived from acrylonitrile-divinylbenzene copolymer. *Chem. Eng. J.* 187, 193–202. doi: 10.1016/j.cej.2012.01.120
- Eskandarpour, A., Onyango, M. S., Ochieng, A., and Asai, S. (2008). Removal of fluoride ions from aqueous solution at low pH using schwertmannite. *J. Hazard. Mater.* 152, 571–579. doi: 10.1016/j.jhazmat.2007.07.020
- Gorzin, F., and Bahri Rasht Abadi, M. M. (2018). Adsorption of Cr (VI) from aqueous solution by adsorbent prepared from paper mill sludge: kinetics and thermodynamics studies. *Adsorp. Sci. Technol.* 36, 149–169. doi: 10.1177/0263617416686976
- Hamdaoui, O., and Naffrechoux, E. (2007). Modeling of adsorption isotherms of phenol and chlorophenols onto granular activated carbon: part I. Two-parameter models and equations allowing determination of thermodynamic parameters. *J. Hazard. Mater.* 147, 381–394. doi: 10.1016/j.jhazmat.2007.01.021
- Hu, S., Guan, Y., Wang, Y., and Han, H. (2011). Nano-magnetic catalyst KF/CaO–Fe₃O₄ for biodiesel production. *Appl. Energy* 88, 2685–2690. doi: 10.1016/j.apenergy.2011.02.012
- Huang, G., Shi, J. X., and Langrish, T. A. (2009). Removal of Cr (VI) from aqueous solution using activated carbon modified with nitric acid. *Chem. Eng. J.* 152, 434–439. doi: 10.1016/j.cej.2009.05.003
- Huang, Y. D. (2019). Comments on using of “pseudo-first-order model” [Appl. Surf. Sci. 394 (2017) 378–385, 397 (2017) 133–143, 426 (2017) 545–553, 437 (2018) 294–303]. *Appl. Surf. Sci.* 469, 564–565. doi: 10.1016/j.apsusc.2018.11.070
- Kalidhasan, S., Kumar, A. S. K., Rajesh, V., and Rajesh, N. (2016). The journey traversed in the remediation of hexavalent chromium and the road ahead toward greener alternatives—a perspective. *Coord. Chem. Rev.* 317, 157–166. doi: 10.1016/j.ccr.2016.03.004
- Kera, N. H., Bhaumik, M., Pillay, K., Ray, S. S., and Maity, A. (2017). Selective removal of toxic Cr (VI) from aqueous solution by adsorption combined with reduction at a magnetic nanocomposite surface. *J. Colloid Interf. Sci.* 503, 214–228. doi: 10.1016/j.jcis.2017.05.018
- Krishna, P. G., Gladis, J. M., Rambabu, U., Rao, T. P., and Naidu, G. R. K. (2004). Preconcentrative separation of chromium (VI) species from chromium (III) by coprecipitation of its ethyl xanthate complex onto naphthalene. *Talanta* 63, 541–546. doi: 10.1016/j.talanta.2003.11.032
- Krishnani, K. K., Srinives, S., Mohapatra, B. C., Boddu, V. M., Hao, J., Meng, X., et al. (2013). Hexavalent chromium removal mechanism using conducting polymers. *J. Hazard. Mater.* 252, 99–106. doi: 10.1016/j.jhazmat.2013.01.079
- Kurniawan, T. A., Chan, G. Y., Lo, W. H., and Babel, S. (2006). Physico-chemical treatment techniques for wastewater laden with heavy metals. *Chem. Eng. J.* 118, 83–98. doi: 10.1016/j.cej.2006.01.015
- Leyva-Ramos, R., Bernal-Jacome, L. A., and Acosta-Rodriguez, I. (2005). Adsorption of cadmium (II) from aqueous solution on natural and oxidized corncob. *Separat. Purif. Technol.* 45, 41–49. doi: 10.1016/j.seppur.2005.02.005
- Liu, Y., Li, Y., Hu, Y., Mostofa, K. M., Li, S., and Liu, Z. (2019). Adsorption characteristics and transport behavior of Cr (VI) in shallow aquifers surrounding a chromium ore processing residue (COPR) dumpsite. *J. Chem.* 2019. doi: 10.1155/2019/4932837
- Malkoc, E. (2006). Ni (II) removal from aqueous solutions using cone biomass of Thuja orientalis. *J. Hazard. Mater.* 137, 899–908. doi: 10.1016/j.jhazmat.2006.03.004
- Masekela, D., Hintsho-Mbita, N. C., and Mabuba, N. (2020). Diethylamine functionalised Moringa oleifera leaves for the removal of chromium (VI) and bacteria from wastewater. *Int. J. Environ. Anal. Chem.* 1–21. doi: 10.1080/03067319.2020.1762873
- Murcia-Salvador, A., Pellicer, J. A., Fortea, M. I., Gómez-López, V. M., Rodríguez-López, M. I., Núñez-Delgado, E., et al. (2019). Adsorption of Direct Blue 78 using chitosan and cyclodextrins as adsorbents. *Polymers* 11, 1003. doi: 10.3390/polym11061003
- Nejadshafie, V., and Islami, M. R. (2019). Adsorption capacity of heavy metal ions using sultone-modified magnetic activated carbon as a bio-adsorbent. *Mater. Sci. Eng. C* 101, 42–52. doi: 10.1016/j.msec.2019.03.081
- Nguyen, T. A. H., Ngo, H. H., Guo, W. S., Zhang, J., Liang, S., Yue, Q. Y., et al. (2013). Applicability of agricultural waste and by-products for adsorptive removal of heavy metals from wastewater. *Bioresour. Technol.* 148, 574–585. doi: 10.1016/j.biortech.2013.08.124
- Niu, J., Ding, P., Jia, X., Hu, G., and Li, Z. (2019). Study of the properties and mechanism of deep reduction and efficient adsorption of Cr (VI) by low-cost Fe₃O₄-modified ceramsite. *Sci. Total Environ.* 688, 994–1004. doi: 10.1016/j.scitotenv.2019.06.333
- Oliveira, W. E., Franca, A. S., Oliveira, L. S., and Rocha, S. D. (2008). Untreated coffee husks as biosorbents for the removal of heavy metals from aqueous solutions. *J. Hazard. Mater.* 152, 1073–1081. doi: 10.1016/j.jhazmat.2007.07.085
- Ou, B., Wang, J., Wu, Y., Zhao, S., and Wang, Z. (2020). Efficient removal of Cr (VI) by magnetic and recyclable calcined CoFe-LDH/g-C₃N₄ via the synergy of adsorption and photocatalysis under visible light. *Chem. Eng. J.* 380, 122600. doi: 10.1016/j.cej.2019.122600
- Panneerselvam, P., Morad, N., and Tan, K. A. (2011). Magnetic nanoparticle (Fe₃O₄) impregnated onto tea waste for the removal of nickel (II) from aqueous solution. *J. Hazard. Mater.* 186, 160–168. doi: 10.1016/j.jhazmat.2010.10.102
- Pellerin, C., and Booker, S. M. (2000). Reflections on hexavalent chromium: health hazards of an industrial heavyweight. *Environ. Health Perspect.* 108, A402–A407. doi: 10.1289/ehp.108-a402
- Peng, X., Hu, F., Zhang, T., Qiu, F., and Dai, H. (2018). Amine-functionalized magnetic bamboo-based activated carbon adsorptive removal of ciprofloxacin and norfloxacin: a batch and fixed-bed column study. *Bioresour. Technol.* 249, 924–934. doi: 10.1016/j.biortech.2017.10.095
- Periyasamy, S., Manivasakan, P., Jayaprabha, C., Meenakshi, S., and Viswanathan, N. (2019). Fabrication of nano-graphene oxide assisted hydrotalcite/chitosan biocomposite: an efficient adsorbent for chromium removal from water. *Int. J. Biol. Macromol.* 132, 1068–1078. doi: 10.1016/j.ijbiomac.2019.03.232
- Popoola, L. T. (2019). Nano-magnetic walnut shell-rice husk for Cd (II) sorption: design and optimization using artificial intelligence and design expert. *Heliyon* 5, e02381. doi: 10.1016/j.heliyon.2019.e02381
- Saha, R., Nandi, R., and Saha, B. (2011). Sources and toxicity of hexavalent chromium. *J. Coord. Chem.* 64, 1782–1806. doi: 10.1080/00958972.2011.583646
- Sasikala, S., and Muthuraman, G. (2015). Chromium (VI) removal using biosorbents derived from Moringa oleifera. *Ind. Chem. Open Access* 1, 2. doi: 10.4172/2469-9764.1000105
- Shirani, Z., Santhosh, C., Iqbal, J., and Bhatnagar, A. (2018). Waste Moringa oleifera seed pods as green sorbent for efficient removal of toxic aquatic pollutants. *J. Environ. Manag.* 227, 95–106. doi: 10.1016/j.jenvman.2018.08.077
- Timbo, C. C., Kandawa-Schulz, M., Amuanyena, M., and Kwaambwa, H. M. (2017). Adsorptive removal from aqueous solution of Cr (VI) by green moringa tea leaves biomass. *J. Encapsul. Adsorpt. Sci.* 7, 108–119. doi: 10.4236/jeas.2017.72008
- Wan, M. W., Kan, C. C., Rogel, B. D., and Dalida, M. L. P. (2010). Adsorption of copper (II) and lead (II) ions from aqueous solution on chitosan-coated sand. *Carbohydr. Polym.* 80, 891–899. doi: 10.1016/j.carbpol.2009.12.048
- Wang, J., Liu, G., Li, T., and Zhou, C. (2015). Physicochemical studies toward the removal of Zn (II) and Pb (II) ions through adsorption on montmorillonite-supported zero-valent iron nanoparticles. *RSC Adv.* 5, 29859–29871. doi: 10.1039/C5RA02108A
- Wartelle, L. H., and Marshall, W. E. (2006). Quaternized agricultural by-products as anion exchange resins. *J. Environ. Manag.* 78, 157–162. doi: 10.1016/j.jenvman.2004.12.008
- Yusuf, A. M., and Malek, N. A. N. N. (2009). Removal of Cr (VI) and As (V) from aqueous solutions by HDTMA-modified zeolite Y. *J. Hazard. Mater.* 162, 1019–1024. doi: 10.1016/j.jhazmat.2008.05.134
- Zainol, M. M., Asmadi, M., and Amin, N. A. S. (2015). Impregnation of magnetic particles on oil palm shell activated carbon for removal of heavy metal ions from aqueous solution. *J. Teknol.* 72. doi: 10.11113/jt.v72.3278

Zarringhalam, M., Ahmadi-Danesh-Ashtiani, H., Toghraie, D., and Fazaeli, R. (2019). The effects of suspending Copper nanoparticles into Argon base fluid inside a microchannel under boiling flow condition by using of molecular dynamic simulation. *J. Mol. Liquids* 293, 111474. doi: 10.1016/j.molliq.2019.111474

Conflict of Interest: The authors declare that the research was conducted in the absence of any commercial or financial relationships that could be construed as a potential conflict of interest.

Publisher's Note: All claims expressed in this article are solely those of the authors and do not necessarily represent those of their affiliated organizations, or those of

the publisher, the editors and the reviewers. Any product that may be evaluated in this article, or claim that may be made by its manufacturer, is not guaranteed or endorsed by the publisher.

Copyright © 2022 Masekela, Yusuf, Hintshe-Mbita and Mabuba. This is an open-access article distributed under the terms of the Creative Commons Attribution License (CC BY). The use, distribution or reproduction in other forums is permitted, provided the original author(s) and the copyright owner(s) are credited and that the original publication in this journal is cited, in accordance with accepted academic practice. No use, distribution or reproduction is permitted which does not comply with these terms.